Soft-Switching Technique for A Three-Phase Bidirectional Grid-Tie DC-AC-AC Converter

Mahmoud A. Sayed mahmoud_sayed@ieee.org
Kazuma Suzuki 26417571@stn.nitech.ac.jp
Takaharu Takeshita take@nitech.ac.jp
Wataru Kitagawa kitagawa.wataru@nitech.ac.jp
Department of Electrical and Mechanical Engineering, Nagoya Institute of Technology,
466-8555, Showa-ku, Gokiso, Nagoya, JAPAN.

***Abstract*—This paper presents a new mathematical model and a soft-switching technique for the bidirectional three-phase grid-tie DC-AC-AC converter of the matrix converter high-frequency link type. The converter topology consists of a conventional H-bridge circuit linked to a single-phase-to-three-phase matrix converter through a single-phase high-frequency transformer (HFT). The proposed control technique regulates battery current and injects three-phase sinusoidal current to grid at unity power factor. The proposed mathematical model uses a trapezoidal approximation of the high-frequency (HF) current to obtain the accurate duty cycles for all matrix converter switches, which results in low total harmonic distortion (THD) at the grid side. Also, the proposed soft-switching technique enhances the system overall efficiency. Moreover, using HFT as a galvanic isolation between the battery and grid sides enhances the system efficiency and reduces the overall size and weight. The mathematical model of the DC-AC-AC converter and the circuit operational modes for soft-switching are presented along with the voltage controllable limits. The system validity has been verified experimentally using laboratory prototype.**

Keywords*—*DC-AC-AC converter, grid-tie bidirectional DC-AC converter, Pulse Width Modulation (PWM), High-Frequency Transformer (HFT), soft-switching.

I. Introduction

Concerns over energy crisis and global warming have led to a significant amount of research on renewable energy systems and the methods facilitating their grid integration [1]–[3]. The generated power of these sources is continuously varying according to the weather. Therefore, incorporation of energy storage devices, such as batteries, in distributed generation systems is essential in order to smooth out active power flow on the utility grid by storing the excess energy and retrieve it back when needed [4]. Consequently, the need for high efficiency, high reliability, and high power density DC-AC bidirectional converters has been treated extensively in the literature [5]. The bidirectional converters enables power to flow in both directions between the grid and the batteries [6].

A simple technique was proposed in [7] for a line commutated controlled rectifier that can operate in the inversion mode by adjusting its delay angle. However, it has poor power factor at the grid side, high Total Harmonic Distortion (THD), and low efficiency. On the other hand, the bidirectional three-phase Voltage Source Inverter (VSI) has a good dynamic performance and injects a sinusoidal AC current to the grid at unity power factor [5], [8], [9]. An LC filter is installed at the grid side to eliminate the high-frequency components. In [10], [11], matrix converter is proposed as a bidirectional AC-DC converter. However, the grid-tie AC-DC converters based on VSI or matrix converter need bulky transformers for galvanic isolation between the AC and DC sides, which increase the system size and weight. Also, transformer reduces the overall efficiency due to its high leakage inductance. Moreover, the VSI generally requires PLL or hysteresis current controller for synchronizing the inverter output frequency with the grid [7].

Recently, HFT has been emerged as an alternative to the conventional bulky transformer operating in line frequency (50/60 Hz) for galvanic isolation between the AC and DC sides [12], [13]. Therefore, bidirectional DC-AC converter with HFT has the merits of high efficiency and high power density [14]. It can be classified into two types [15]–[17]. The first one is the rectifier HF link that has a Voltage Source Inverter (VSI) linked with a Dual Active Bridge (DAB) through a common DC-link capacitor [18]. However, it utilizes an additional converter stage with a bulky short life-time capacitor. The second one is the matrix converter HF link that uses matrix converter linked with an H-bridge through a single-phase HFT [14], [19]. It has the merits of high power density since it get rid of the bulky DC-link capacitor.

This paper proposes a new mathematical model and a PWM switching technique for controlling the three-phase bidirectional grid-tie DC-AC-AC converter of the matrix converter high-frequency link type. The new mathematical model provides the matrix converter switches with their accurate duty cycles. On the other hand, the PWM switching technique of the matrix converter minimizes the number of switching transitions, which enhances the system efficiency. Moreover, soft-switching technique has been achieved by using a shunt ceramic capacitor with each bidirectional switch of the matrix converter and each switch of the H-bridge converter. Therefore, this system has the merits of high power density, high efficiency and low THD. A detailed mathematical model of the DC-AC-AC converter, PWM switching technique, and the soft-switching operational modes have been presented. The effectiveness of the proposed mathematical model in addition to the soft-switching technique has been verified experimentally.

II. Configuration of the DC-AC-AC converter

Fig. 1 shows the circuit configuration of the two-stage bidirectional three-phase grid-tie DC-AC-AC converter of the matrix converter high-frequency link type. In the first stage,

978-1-5386-1180-7/18/$31.00 ©2018 IEEE

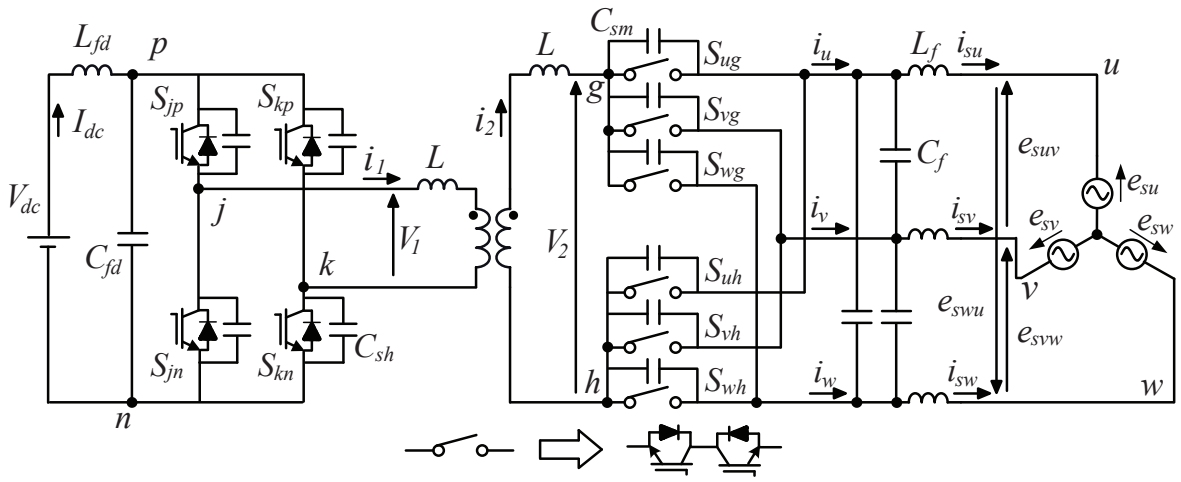

Fig. 1: System configuration of the DC-AC-AC converter.

a single-phase H-bridge converter is used to convert the DC voltage to a single-phase HF square-wave. In the second stage, a direct three-phase to single-phase matrix converter is used to convert the HF voltage to three-phase waveforms synchronized with the grid. Therefore, a single-phase HFT is used to link the H-bridge and the matrix converters. A smoothing inductor L is installed to smooth the current waveforms at the HFT. Also, LC filters are installed at battery and grid sides to eliminate the HF components of the currents. Therefore, the parameters of both LC filters are usually small. For soft-switching, a shunt ceramic capacitor is connected with each switch of the H-bridge converter and each bidirectional switch of the matrix converter.

III. PWM Switching Pattern

Fig. 2 shows the PWM switching pattern in addition to the output voltage and current waveforms of the converter. The switching pattern of the matrix converter is explained during the time of $(\pi/6 < \theta < \pi/3)$, when the levels of the three-phase grid voltages are $e_{su} > e_{sv} > 0 > e_{sw}$. Bipolar PWM switching technique is used for the H-bridge converter, hence the output voltage v_1 has two levels of $\pm V_{dc}$. In the positive half-cycle of the matrix converter output voltage v_2, terminal g is switched with all three-phase grid voltages, whereas terminal h is connected only with the minimum phase voltage w. In the negative half-cycle, the switching process is reversed. Therefore, the output voltage v_2 has three-levels; (i.e.; zero and $\pm$ signals of the line-to-line grid voltages). Although matrix converter has six bidirectional switches, the commutations in each control period are only three, which enhances the converter efficiency. The detailed switching pattern and PWM switching signals of all switches are presented in [17], [20].

Fig. 3 shows the PWM technique and the related gate signals of each switch in the H-bridge converter and each bidirectional switch in the matrix converters, based on the grid line-to-line voltages and the reference input currents of the matrix converter. It also shows the input current waveform i_u of the matrix converter in addition to the primary and secondary voltages of the HFT (i.e.; v_1 and v_2).

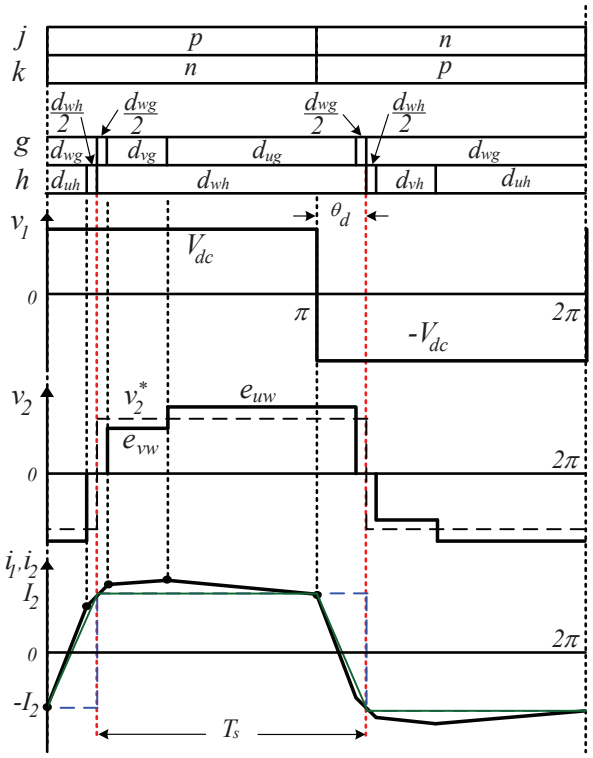

Fig. 2: Switching pattern of the DC-AC-AC converter.

IV. Modeling and Duty Cycles of the Matrix Converter

The three-phase grid voltages e_{su}, e_{sv}, and e_{sw} are given using the rms line voltage E and the displacement angle θ as

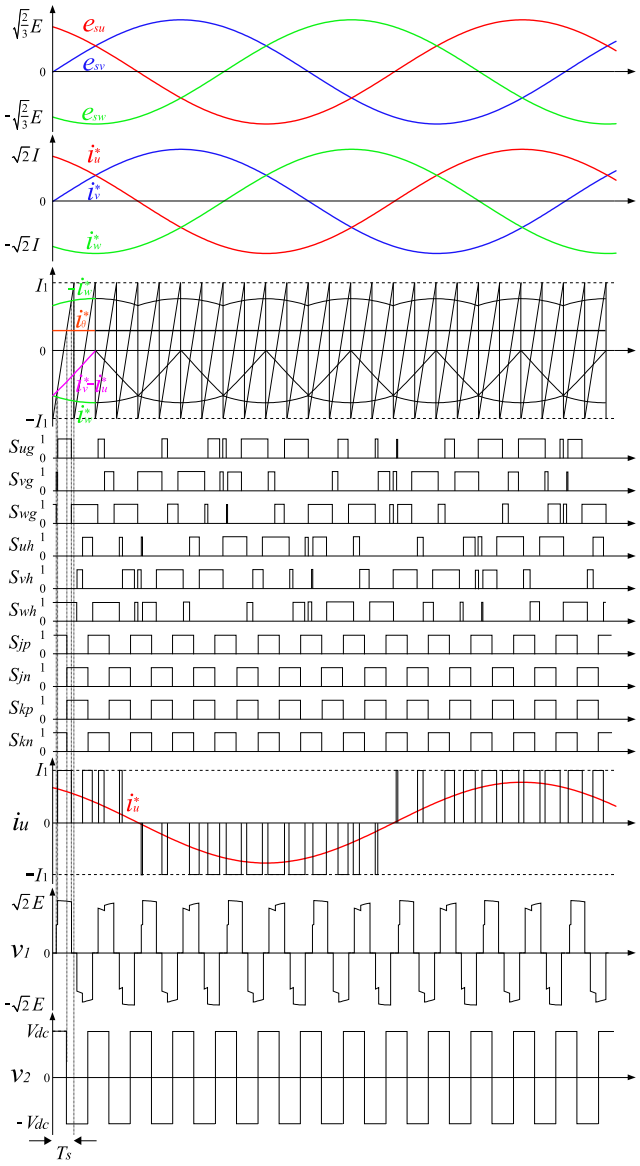

Fig. 3: Detailed PWM switching signals of the DC-AC-AC converter.

follows:

$$\begin{bmatrix} e_{su} \\ e_{sv} \\ e_{sw} \end{bmatrix} = \sqrt{\frac{2}{3}}E \begin{bmatrix} \cos\theta \\ \cos(\theta - 2\pi/3) \\ \cos(\theta + 2\pi/3) \end{bmatrix} \tag{1}$$

where

$$\theta = \omega t \tag{2}$$

where ω is the angular frequency of the three-phase grid voltage. The grid line-to-line voltages e_{suv}, e_{svw}, and e_{swu} can be formulated as follows:

$$\begin{bmatrix} e_{suv} \\ e_{svw} \\ e_{swu} \end{bmatrix} = \begin{bmatrix} e_{su} - e_{sv} \\ e_{sv} - e_{sw} \\ e_{sw} - e_{su} \end{bmatrix} = \sqrt{2}E \begin{bmatrix} \cos(\theta + \pi/6) \\ \cos(\theta - \pi/2) \\ \cos(\theta - 7\pi/6) \end{bmatrix} \tag{3}$$

Considering unity power factor at the grid side, the reference grid injected currents i_u^*, i_v^*, and i_w^* can be formulated as follows:

$$\begin{bmatrix} i_u^* \\ i_v^* \\ i_w^* \end{bmatrix} = \sqrt{2}I \begin{bmatrix} \cos(\theta + \varphi^*) \\ \cos(\theta - 2\pi/3 + \varphi^*) \\ \cos(\theta - 4\pi/3 + \varphi^*) \end{bmatrix} \tag{4}$$

where

$$\varphi^* = 0 \tag{5}$$

A. Duty cycles of the matrix converter

All duty cycles $d_{ug} - d_{wh}$ of the matrix converter bidirectional switches should be decided to realize the reference injected current at unity power factor. All switches duty cycles can be formulated based on the following constraints:

$$d_{ug} + d_{vg} + d_{wg} = 1 \tag{6}$$

$$d_{uh} + d_{vh} + d_{wh} = 1 \tag{7}$$

The input power of the matrix converter p_{mc-in} can be formulated as follows:

$$p_{mc-in} = e_{su}i_u^* + e_{sv}i_v^* + e_{sw}i_w^* = \sqrt{3}EI\cos\varphi^* \tag{8}$$

On the other hand, the matrix converter output power p_{mc-out} can be formulated as follows:

$$p_{mc-out} = v_2 i_2 \tag{9}$$

Owing to its galvanic isolation function, HFT has a 1:1 turns ratio. Therefore, the primary and secondary currents are same (i.e.; $i_1 = i_2$). Also, the primary and secondary voltages equal the battery dc voltage; (i.e.; $v_1 = v_2^* = V_{dc}$). For simplification, the HF current i_2 can be approximated to either a square-wave or a trapezoidal waveform, as shown by the blue-dotted line and the green-solid line, respectively, with the current waveform in Fig. 2. The square-wave approximation of the current i_2 results in a considerable error in the duty cycle calculations [14], [17]. The trapezoidal approximation of the current i_2 looks same as the actual one, which results in accurate calculations of the duty cycles [21]. Considering trapezoidal approximation of the current i_2, the matrix converter output power can be expressed as follows:

$$p_{mc-out} = v_2^* i_2 = V_{dc}I_2(1 - \frac{\theta_d}{\pi}) \tag{10}$$

Assuming ideal matrix converter with equal input and output power, the trapezoidal current I_2 can be formulated as:

$$I_2 = \frac{\sqrt{3}EI\cos\varphi^*}{V_{dc}(1 - \frac{\theta_d}{\pi})} \tag{11}$$

Also, the trapezoidal current I_2 can be obtained, based on the current waveform in Fig. 2, as follows:

$$I_2 = \frac{1}{2L}\int_0^{T_s} (v_1^* - v_2^*)\, dt = \frac{V_{dc}\theta_d T_s}{2L\pi} \tag{12}$$

Based on (10), (11) and (12), the phase shift angle θ_d between v_1 and v_2 can be formulated as follows:

$$\theta_d = \frac{\pi \pm \sqrt{\pi^2 - 4K}}{2} \tag{13}$$

where

$$K = \frac{2L\pi^2 p_{mc-out}}{V_{dc}^2 T_s} \tag{14}$$

The matrix converter reference voltage v_2^* can be formulated, based on the switching pattern of Fig. 2, as follows:

$$\begin{aligned} v_2^* &= (d_{ug}–d_{uh})e_{su}+(d_{vg}–d_{vh})e_{sv}+(d_{wg}–d_{wh})e_{sw} \\ &= (d_{ug}-d_{uh})e_{suw}+(d_{vg}-d_{vh})e_{svw} \end{aligned} \tag{15}$$

Considering duty cycles of the matrix converter, the reference current of the matrix converter i_u^*, i_v^*, and i_w^* can be formulated as follows:

$$\left.\begin{aligned} i_u^* &= (d_{ug}-d_{uh})i_2 \\ i_v^* &= (d_{vg}-d_{vh})i_2 \\ i_w^* &= (d_{wg}-d_{wh})i_2 \end{aligned}\right\} \tag{16}$$

Therefore, the average currents of phase u and v (i.e.; $\bar{i_u}$ and $\bar{i_v}$) in each half-cycle of the voltage v_2 can be formulated as follows:

$$\bar{i_u} = \frac{1}{T_s}\int_{T_s(\frac{d_{wg}}{2}+d_{vg})}^{T_s(1-\frac{d_{wg}}{2})} i_2\ dt \simeq (1-\frac{\theta_d}{\pi}-d_{vg})I_2 \tag{17}$$

$$\bar{i_v} = \frac{1}{T_s}\int_{T_s(\frac{d_{wg}}{2})}^{T_s(\frac{d_{wg}}{2}+d_{vg})} i_2\ dt = d_{vg}I_2 \tag{18}$$

In the positive half-cycle of the matrix converter voltage v_2, the switch S_{wh} is always ON during the control period T_s. Therefore, the duty cycles of all switches linked with terminal h (i.e.; d_{uh}, d_{vh}, and d_{wh}) can be formulated as follows:

$$d_{uh}=0,\ d_{vh}=0,\ d_{wh}=1 \tag{19}$$

Considering the reference and average currents of the matrix converter are equal, the duty cycles of all switches linked with terminal g (i.e.; d_{ug}, d_{vg}, and d_{wg}) can be formulated, based on (4), (6), (17), (18) and (19), as follows:

$$d_{ug} = \frac{v_2^* - e_{vw}d_{vg}}{e_{uw}} \tag{20}$$

$$d_{vg} = (1-\frac{\theta_d}{\pi})\frac{i_v^*}{i_u^*+i_v^*} \tag{21}$$

$$d_{wg} = \frac{e_{uw}-v_2^*-e_{uv}d_{vg}}{e_{uw}} \tag{22}$$

Likewise, in the negative half-cycle of v_2, the switch S_{wg} is always ON during the control period T_s. Therefore, the duty cycles of all switches linked with terminal g (i.e.; d_{ug}, d_{vg}, and d_{wg}) can be formulated as follows:

$$d_{ug}=0,\ d_{vg}=0,\ d_{wg}=1 \tag{23}$$

Based on (4), (7), (17), (18) and (23), the duty cycles of all switches linked with terminal h (i.e.; d_{uh}, d_{vh}, and d_{wh}) can be formulated as follows:

$$d_{uh} = \frac{v_2^* - e_{vw}d_{vh}}{e_{uw}} \tag{24}$$

$$d_{vh} = (1-\frac{\theta_d}{\pi})\frac{i_v^*}{i_u^*+i_v^*} \tag{25}$$

$$d_{wh} = \frac{e_{uw}-v_2^*-e_{uv}d_{vh}}{e_{uw}} \tag{26}$$

B. Control limits of the matrix converter

To avoid over modulation and to satisfy the duty cycle constraints in (6) and (7), the limits of the reference voltage v_2^* of the matrix converter should be determined based on the duty cycle d_{wg}, given in (22), as follows:

$$d_{ug}+d_{vg} = 1-\frac{e_{uw}-v_2^*-e_{uv}d_{vg}}{e_{uw}} \le 1 \tag{27}$$

Considering $\varphi^*=0$ and $\pi/6<\theta<\pi/3$, the limit of v_2^* can be obtained as follows:

$$v_2^* \le \sqrt{\frac{3}{2}}E \quad , \quad (\varphi^*=0,\ \theta=\pi/3) \tag{28}$$

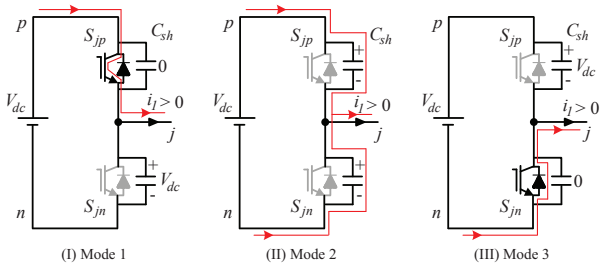

Fig. 4: Soft-switching of the H-bridge converter.

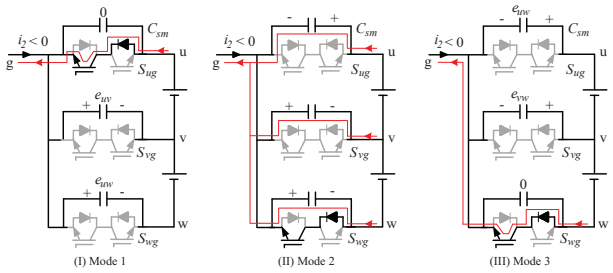

Fig. 5: Soft-switching of the matrix converter.

V. Proposed Soft-switching Technique

Soft-switching techniques for power electronics devices are used to reduce the switching losses and noise issues, which in-turn enhances the converter efficiency. These techniques are usually switching ON or OFF the power semiconductors at zero voltage resulting in zero-voltage switching (ZVS). Other techniques are usually switching the power semiconductors ON or OFF at zero current resulting in zero-current switching (ZCS) [22]–[26].

Fig. 4 and Fig. 5 show the proposed soft-switching technique of the H-bridge and matrix converters, respectively. In the H-bridge converter, a shunt ceramic capacitor C_{sh} is connected with each switch to provide ZVS for all ON-coming switches and ZCS for all OFF-going switches. Likewise, in the matrix converter, a shunt ceramic capacitor C_{sm} is connected with each bidirectional switch to provide ZVS for all ON-coming switches and ZCS for all OFF-going switches. The

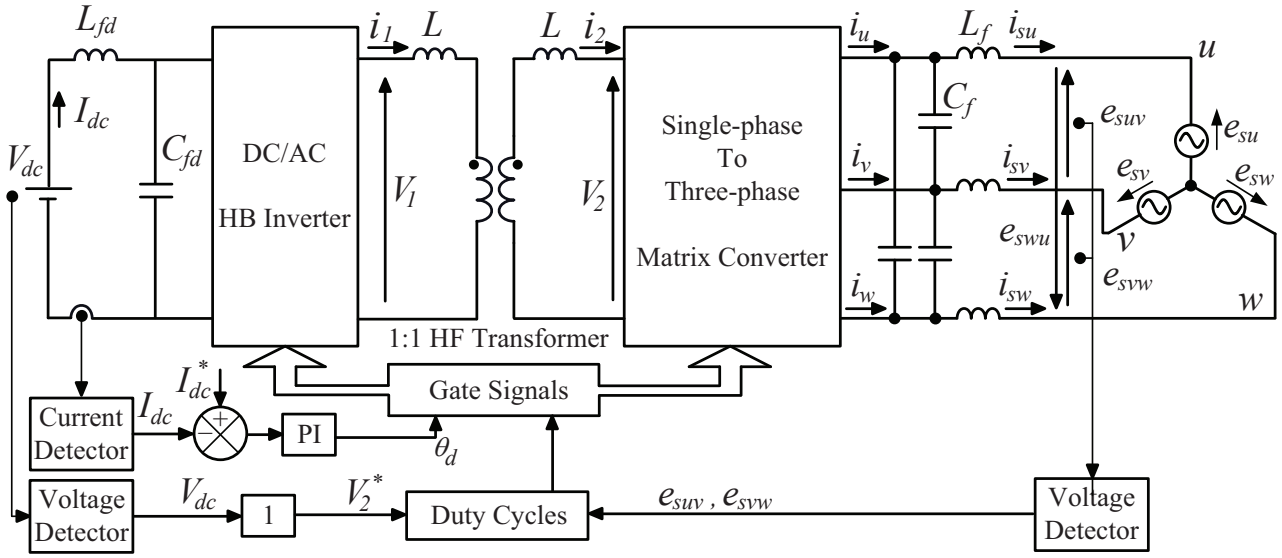

Fig. 6: Experimental system configuration.

proposed soft-switching technique has been designed based on the current direction of the HFT, shown in Fig. 2 . Also, the current transition in both H-bridge and matrix converters has similar three modes of operation, as shown in Fig. 4 and Fig. 5 . In both figures, the red-solid line direction represents the current path in the OFF-going switches, whereas the red-dotted line direction represents the current path in the ON-coming switches. In mode 1, the current flows in the OFF-going switch. In mode 2, the current transits from the OFF-going switch to the soft-switching capacitors providing ZCS. In mode 3, the current transits from the soft-switching capacitors to the ON-coming switch providing ZVS. Obviously, The OFF-going switch is shunted with a zero-voltage capacitor that provides ZCS, whereas the ON-coming switch is shunted with a charged capacitor that provides ZVS by bypassing switch current. In order to avoid circulating current between the discharging capacitor and the ON-coming switch, soft-switching capacitors must be fully discharged within the dead-time T_{dead} between the OFF-going and ON-coming switches.

Fig. 4 shows the soft-switching technique for each leg of the H-bridge converter. It is clear that the shunt ceramic capacitor C_{sh} across each switch of the H-bridge converter provides an alternative path for the current to realize ZVS or ZCS. Based on the direction of the HFT current i_1, the current transition in each leg of the H-bridge converter can be considered as follows:

$$\begin{cases} S_{jp} \rightarrow S_{jn}, & i_1 > 0 \\ S_{jn} \rightarrow S_{jp}, & i_1 < 0 \end{cases} \tag{29}$$

According to the grid three-phase voltage levels ($e_{su} > e_{sv} > 0 > e_{sw}$) during the period of ($\pi/6 < \theta < \pi/3$) in addition to the switching pattern and the HFT current waveform i_1 shown in Fig. 2 , operational sequence of the matrix converter bidirectional switches, connecting terminal g with the grid, is $S_{wg} \rightarrow S_{vg} \rightarrow S_{ug} \rightarrow S_{wg}$. In this case, the current transition between the bidirectional switches of the matrix converter can be considered as follows:

$$\begin{cases} S_{wg} \rightarrow S_{vg} & (e_w < e_v), \quad i_2 > 0 \\ S_{vg} \rightarrow S_{ug} & (e_v < e_u), \quad i_2 > 0 \\ S_{ug} \rightarrow S_{wg} & (e_u > e_w), \quad i_2 < 0 \end{cases} \tag{30}$$

Using the information of the phase shift angle θ_d between the primary and secondary voltages of the HFT in addition to the dead time T_{dead} between the OFF-going and ON-coming switches, the capacitance C_{sh} of each soft-switching capacitor across each switch of the H-bridge converter can be formulated as follows:

$$C_{sh} \leq \frac{T_{dead}}{8LV_{dc}}(T_s(V_{dc} - e_{vw}d_{vg} + e_{uw}(d_{vg} + \frac{2\theta_d}{\pi} - 1)) - T_{dead}(V_{dc} + e_{uw})) \tag{31}$$

Also, the capacitance C_{sm} of each soft-switching capacitor across each bidirectional switch of the matrix converter can be formulated as follows:

$$C_{sm} \leq \frac{T_{dead}}{12Le_{uw}}(T_{dead}V_{dc} - T_s(V_{dc}(1 + d_{wg} - \frac{2\theta_d}{\pi}) - e_{uw}d_{ug} - e_{vw}d_{vg})) \tag{32}$$

VI. Experimental Results

A. System configuration and control technique

Fig. 6 shows the configuration of the laboratory prototype of the bidirectional three-phase grid-tie DC-AC-AC converter of the matrix converter HFL type. The H-bridge converter is used to convert the battery dc voltage to square-waveform with 50% duty cycle. On the other hand, the matrix converter is used to convert the grid three-phase voltage to a single-phase quasi square-waveform. The H-bridge and matrix

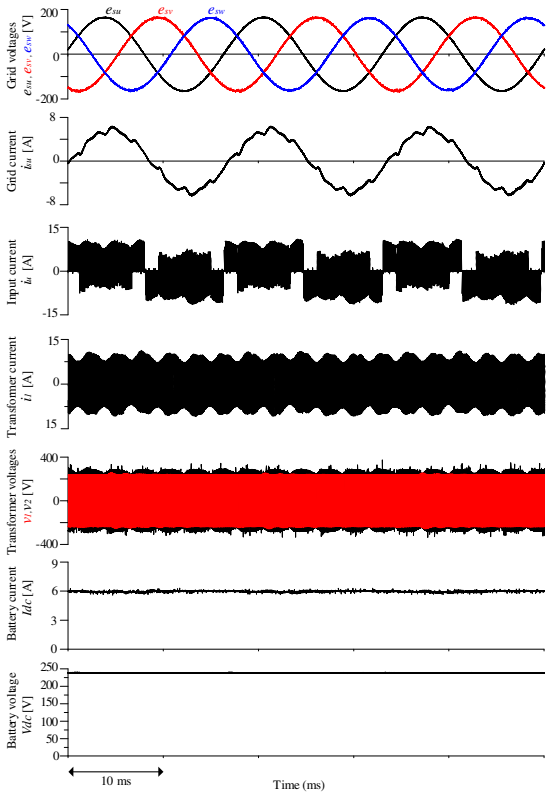

Fig. 7: Experimental results of Case-I.

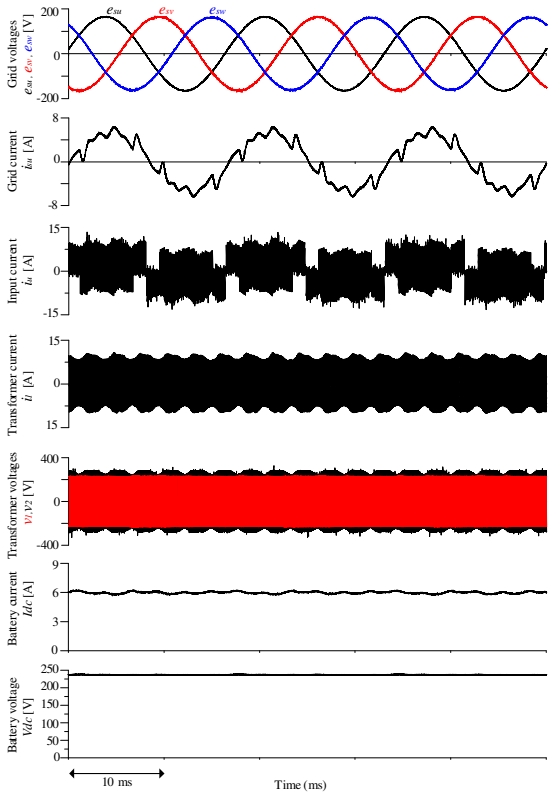

Fig. 8: Experimental results of Case-II.

TABLE I: Experimental system parameters

Grid voltage E, ω	200V , 2 $\pi\times$ 60 rad/s
Power factor angle φ^*	0 rad
DC battery voltage V_{dc}^*	240 V
DC current reference I_{dc}^*	6.0 A
Power P_{out}	1440 W
Grid filter L_f, C_f	1.2 mH , 7.1μF
Battery filter L_{fd}, C_{fd}	3 mH , 300μF
Transformer turn ratio $N_1 : N_2$	1 : 1
Inductors L	0.2 mH
Capacitors C_{sm}, C_{sh}	0.5 nF , 3 nF
Switching frequency	20 kHz

converters are linked by a single-phase HFT with 1:1 turns ratio. Grid and battery are connected to the converter through LC filters to eliminate the high-frequency components of the current. Smoothing inductors L are installed in the primary and secondary sides of the HFT to smooth the HF current waveform. The reference dc current I_{dc}^* is 6.0 A, hence the system capacity is about 1440 W. The system parameters are listed in Table I. The power switches of the H-bridge and matrix converters are implemented by the N-channel SiC power MOSFET C2M0040120D.

B. System results

The laboratory prototype system shown in Fig. 6 has been carried out based on a reference dc current of 6.0 A. Two approximation techniques have been considered for the HFT current in order to simplify the matrix converter duty cycles. In Case-I, the HFT current is approximated to a trapezoidal waveform, whereas in case-II the HFT current is approximated to square waveform. Fig. 7 and Fig. 8 show the experimental results of the system considering Case-I and Case-II; (i.e.; trapezoidal and square-wave approximation techniques of the HF current, respectively). Both figures show the experimental results of the grid three-phase voltage waveforms e_{su}, e_{sv} and e_{sw}, injected grid ac line current i_{su}, matrix converter output current before the LC filter i_u, HFT input current i_1, HFT input and output voltages v_1 and v_2, battery dc current I_{dc}, and battery dc voltage V_{dc}. In both cases, the actual dc current matches the reference one of 6.0 A. Also, the transformer input and output voltages v_1 and v_2 in addition to their related currents i_1 and i_2 are HF waveforms of 10 kHz. In addition, the grid current and phase voltage (i.e.; i_{su} and e_{su}) are in-phase confirming unity power factor at the grid side. However, there is a small phase shift angle error between the grid phase voltage e_{su} and grid injected current i_{su} due to the LC filter. It is clear that the grid current in Case-I is better than that of Case-II. Fig. 9 and Fig. 10 show the FFT spectrum of the grid current in Case-I and Case-II, respectively. The THD is about 7% in Case-I with trapezoidal current approximation, whereas

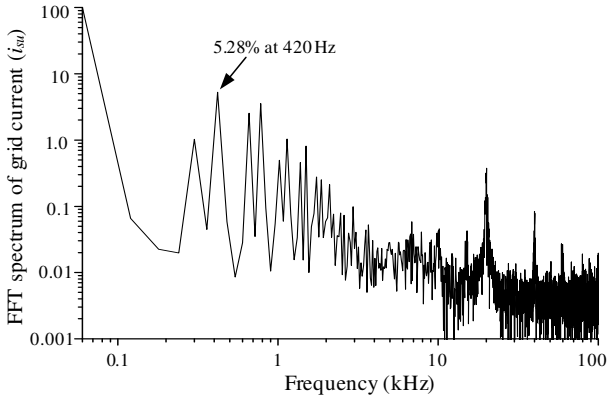

Fig. 9: FFT of grid current in Case-I.

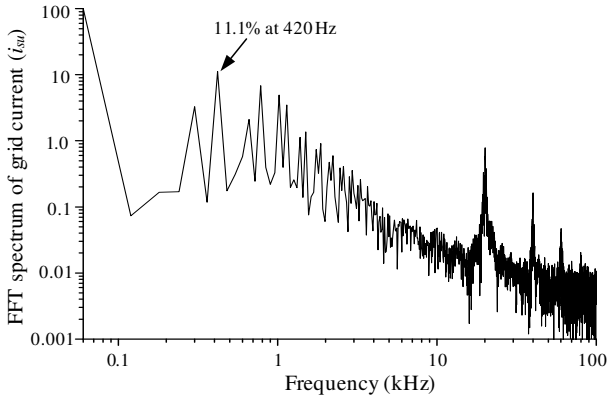

Fig. 10: FFT of grid current in Case-II.

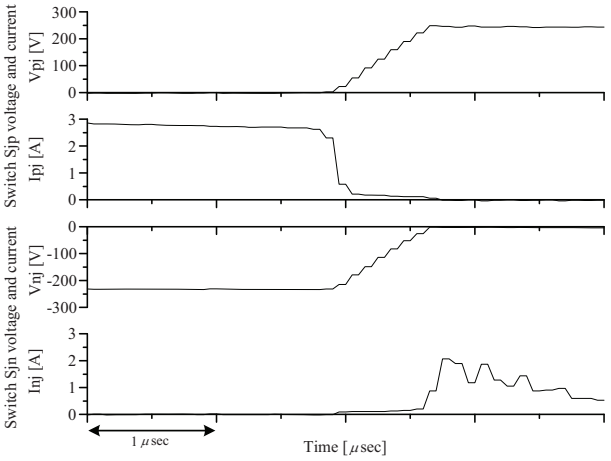

Fig. 11: Soft-switching of H-bridge converter.

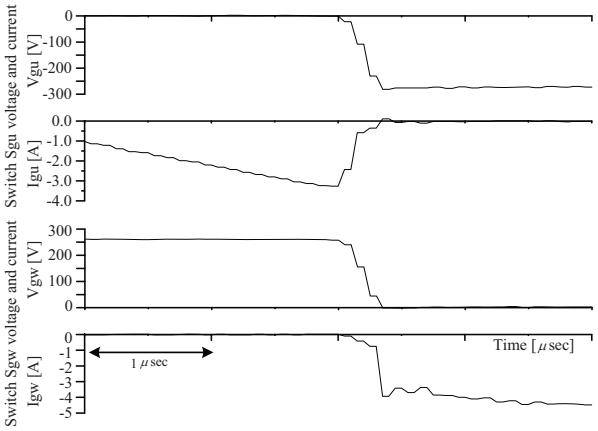

Fig. 12: Soft-switching of matrix converter.

the THD is 14.5% in Case-II with square-wave approximation.

Fig. 11 shows the experimental results of the voltage and current waveforms across the switches S_{jp} and S_{jn} of the H-bridge converter. It depicts the current transition instant from S_{jp} to S_{jn} when switch S_{jp} is OFF-going and switch S_{jn} is ON-coming. Obviously, the current flows from terminal p to terminal j before turning OFF the switch S_{jp}, whereas the current flows from terminal n to terminal j after turning ON the switch S_{jn}. It is clear that the soft-switching is realized in both switches. Therefore, in the H-bridge converter, soft-switching capacitor C_{sh} provides ZCS for the OFF-going switch S_{jp} and ZVS for the ON-coming switch S_{jn}.

In addition, Fig. 12 shows the experimental results of the voltage and current waveforms across the bidirectional switches S_{ug} and S_{wg} of the matrix converter. It depicts the current transition instant from S_{ug} to S_{wg} when switch S_{ug} is OFF-going and switch S_{wg} is ON-coming. Obviously, the current flows from terminal g to terminal u before turning OFF the switch S_{ug}, whereas the current flows from terminal g to terminal w after turning ON the switch S_{wg}. It is clear that the soft-switching is realized in both bidirectional switches. In the matrix converter, soft-switching capacitor C_{sm} provides ZCS for the OFF-going bidirectional switch S_{gu} and ZVS for the ON-coming one S_{gw}. Yokogawa WT1800 power analyzer is used to measure the system efficiency with and without soft-switching capacitors. In both approximation cases, the system efficiency is 96.9% with the soft-switching capacitors, whereas the efficiency is 96.5% without soft-switching capacitors.

Experimental results of both approximation techniques in Case-I and Case-II prove that the system is stable, and the PWM switching technique regulates the dc battery current to match the reference one. Also, both techniques inject a current to the grid at unity power factor. However, the trapezoidal approximation technique dramatically reduces the THD of the grid current compared with the square-wave approximation technique. Moreover, soft-switching of all switches of the H-bridge and matrix converters has been realized, which enhances the system overall efficiency.

VII. Conclusion

This paper has presented a new mathematical model and a soft-switching technique for the bidirectional three-phase grid-tie DC-AC-AC converter that utilizes HFT for galvanic isolation to link a matrix converter with an H-bridge converter. The proposed mathematical model uses trapezoidal approximation of the HFT current waveform to calculate the accurate duty cycles of all matrix converter switches. Also, the PWM switching technique provides a full control of the battery dc current in addition to achieving unity power factor at the grid side. Moreover, soft-switching technique has been achieved by using shunt ceramic capacitor across each switch of the H-bridge converter and each bidirectional switch of the matrix converter. It provides ZVS for the ON-coming switches and ZCS for the OFF-going switches. Permissible limits of the soft-switching capacitors for the H-bridge and matrix converters have been obtained. The effectiveness of the proposed mathematical model has been investigated experimentally using laboratory prototype. Experimentally, the battery current matches the reference one and the grid injected current is a sinusoidal waveform in-phase with the grid voltage. The THD of the grid injected current in case of trapezoidal approximation is less than that of the square-wave approximation. Also, soft-switching technique enhances the system efficiency.

Acknowledgment

This work was supported by Council for Science, Technology and Innovation (CSTI), Cross-ministerial Strategic Innovation Promotion Program (SIP), "Next-generation power electronics" (funding agency: NEDO).

References

[1] M. F. de Melo, W. D. Vizzotto, P. J. Quintana, A. L. Kirsten, M. A. D. Costa, and J. Garcia, "Bidirectional grid-tie flyback converter applied to distributed power generation and street lighting integrated system," *IEEE Transactions on Industry Applications*, vol. 51, pp. 4709–4717, Nov 2015.

[2] J. Rohten, J. Espinoza, J. Munoz, M. Perez, P. Melin, J. Silva, E. Espinosa, and M. Rivera, "Model predictive control for power converters in a distorted three-phase power supply," *IEEE Transactions on Industrial Electronics*, vol. PP, no. 99, pp. 1–1, 2016.

[3] G. Ortiz, J. Biela, D. Bortis, and J. W. Kolar, "1 megawatt, 20 khz, isolated, bidirectional 12kv to 1.2kv dc-dc converter for renewable energy applications," in *Power Electronics Conference (IPEC), 2010 International*, pp. 3212–3219, June 2010.

[4] S. Inoue and H. Akagi, "A bidirectional dc-dc converter for an energy storage system with galvanic isolation," *IEEE Transactions on Power Electronics*, vol. 22, pp. 2299–2306, Nov 2007.

[5] B. Singh, B. Singh, A. Chandra, K. Al-Haddad, A. Pandey, and D. Kothari, "A review of three-phase improved power quality ac-dc converters," *Industrial Electronics, IEEE Transactions on*, vol. 51, pp. 641–660, June 2004.

[6] B. Feng, H. Lin, and X. Wang, "Modulation and control of ac/dc matrix converter for battery energy storage application," *IET Power Electronics*, vol. 8, no. 9, pp. 1583–1594, 2015.

[7] D. Binu Ben Jose, N. Ammasai Gounden, and J. Ravishankar, "Simple power electronic controller for photovoltaic fed grid-tied systems using line commutated inverter with fixed firing angle," *Power Electronics, IET*, vol. 7, pp. 1424–1434, June 2014.

[8] S.-C. Ahn and D. seok Hyun, "New control scheme of three-phase pwm ac/dc converter without phase angle detection under the unbalanced input voltage conditions," *Power Electronics, IEEE Transactions on*, vol. 17, pp. 616–622, Sep 2002.

[9] S. Hosseini, F. Sedaghati, and M. Sarhangzadeh, "Improved power quality three phase ac-dc converter," in *Electrical Machines and Systems (ICEMS), 2010 International Conference on*, pp. 148–153, Oct 2010.

[10] B. Veerasamy, W. Kitagawa, and T. Takeshita, "Input power factor control of bi-directional ac/dc converter," in *Power Electronics and Drive Systems (PEDS), 2013 IEEE 10th International Conference on*, pp. 1103–1108, April 2013.

[11] Y. Fujishima, W. Kitagawa, and T. Takeshita, "Discharge operation of single-stage buck bi-directional ac/dc converter," in *Future Energy Electronics Conference (IFEEC), 2013 1st International*, pp. 12–17, Nov 2013.

[12] S. Manias and P. D. Ziogas, "A novel sinewave in ac to dc converter with high-frequency transformer isolation," *IEEE Transactions on Industrial Electronics*, vol. IE-32, pp. 430–438, Nov 1985.

[13] H. S. Kim, M. H. Ryu, J. W. Baek, and J. H. Jung, "High-efficiency isolated bidirectional ac-dc converter for a dc distribution system," *IEEE Transactions on Power Electronics*, vol. 28, pp. 1642–1654, April 2013.

[14] M. A. Sayed, K. Suzuki, T. Takeshita, and W. Kitagawa, "Modeling and control of bidirectional isolated battery charging and discharging converter based high-frequency link transformer," in *2016 IEEE 7th International Symposium on Power Electronics for Distributed Generation Systems (PEDG)*, pp. 1–8, June 2016.

[15] S. Weearsinghe, D. J. Thrimawithana, and U. K. Madawala, "Modeling bidirectional contactless grid interfaces with a soft dc-link," *IEEE Transactions on Power Electronics*, vol. 30, pp. 3528–3541, July 2015.

[16] G. Ortiz, D. Bortis, J. W. Kolar, and O. Apeldoorn, "Soft-switching techniques for medium-voltage isolated bidirectional dc/dc converters in solid state transformers," in *IECON 2012 - 38th Annual Conference on IEEE Industrial Electronics Society*, pp. 5233–5240, Oct 2012.

[17] M. A. Sayed, K. Suzuki, T. Takeshita, and W. Kitagawa, "Pwm switching technique for three-phase bidirectional grid-tie dc-ac-ac converter with high-frequency isolation," *IEEE Transactions on Power Electronics*, vol. 33, pp. 845–858, Jan 2018.

[18] J. W. Kolar, U. Drofenik, and F. C. Zach, "Vienna rectifier ii-a novel single-stage high-frequency isolated three-phase pwm rectifier system," *IEEE Transactions on Industrial Electronics*, vol. 46, pp. 674–691, Aug 1999.

[19] D. S. B. Weerasinghe, U. K. Madawala, D. J. Thrimawithana, and D. M. Vilathgamuwa, "A three-phase to single-phase matrix converter based bi-directional ipt system for charging electric vehicles," in *ECCE Asia Downunder (ECCE Asia), 2013 IEEE*, pp. 1240–1245, June 2013.

[20] M. A. Sayed, K. Suzuki, T. Takeshita, and W. Kitagawa, "New pwm technique for grid-tie isolated bidirectional dc-ac inverter based high frequency transformer," in *2016 IEEE Energy Conversion Congress and Exposition (ECCE)*, pp. 1–8, Sept 2016.

[21] M. A. Sayed, K. Suzuki, T. Takeshita, and W. Kitagawa, "Grid-tie isolated bidirectional dc-ac-ac converter based on high frequency transformer with high efficiency and low thd," in *2017 19th European Conference on Power Electronics and Applications (EPE'17 ECCE Europe)*, pp. P.1–P.10, Sept 2017.

[22] K. M. Smith and K. M. Smedley, "Intelligent magnetic-amplifier-controlled soft-switching method for amplifiers and inverters," *IEEE Transactions on Power Electronics*, vol. 13, pp. 84–92, Jan 1998.

[23] K. M. Smith and K. M. Smedley, "Lossless passive soft-switching methods for inverters and amplifiers," *IEEE Transactions on Power Electronics*, vol. 15, pp. 164–173, Jan 2000.

[24] R. Teichmann and J. Oyama, "Arcp soft-switching technique in matrix converters," *IEEE Transactions on Industrial Electronics*, vol. 49, pp. 353–361, Apr 2002.

[25] R. Wang, J. Sabate, Y. Mei, J. Xiao, and S. Chi, "Phase-shift soft-switching power amplifier with lower emi noise," in *2014 IEEE Energy Conversion Congress and Exposition (ECCE)*, pp. 2767–2772, Sept 2014.

[26] M. A. Sayed, K. Suzuki, T. Takeshita, and W. Kitagawa, "Soft-switching pwm technique for grid-tie isolated bidirectional dc-ac converter with sic device," *IEEE Transactions on Industry Applications*, vol. PP, no. 99, pp. 1–1, 2017.